Flow Analysis of Ramjet Engine for Optimized Nose Cone Design

Dr. Avinash Govindraju and Dr. Santosh Kumar
Assistant Professor, Department of Mechanical Engineering
BMS Institute of Technology & Management, Bengaluru, India – 560064
avinash.govindaraju@bmsit.in; santoshkumar@iisc.ac.in

Tarun Pachauri, Kartikay Awasthi, Nihal. U. Shetty, Vipan Singh and Karan Manoj
Department of Mechanical Engineering
BMS Institute of Technology & Management, Bengaluru, India – 560064
tarunpachauri786@gmail.com; 1by18me026@bmsit.in; 1by18me034@bmsit.in;
1by18me062@bmsit.in; karanmanoj13@gmail.com

Abstract

This study aims to understand the effects of variable nose cone geometry on the performance of a ramjet engine. The performance of a Ramjet engine is primarily measured by its critical factors, namely, the pressure recovery ratio and velocity variations. Specifically, the combustion performance and overall efficiency of a ramjet engine depend on the pressure recovery ratio. Design modifications are carried out by using the formulae from the literature and simulations are carried out initially to validate the results from the literature for the specified nose cone angle. Further, the nose cone angle is varied from 6° to 20° with increments of 2°, and its impact on the overall performance and efficiency of the Ramjet engine is analyzed. Variations of pressure recovery ratio along the cowl and ramp surface of the engine are plotted along with their contours to determine the most favorable nose cone angle. Considering the optimal nose cone angle, the concavities are also varied along the ramp of the engine's inlet for a range of 2 mm with increments of around 0.5mm in between them. The best pressure recovery ratio which benefits the working of the engine is understood. Graphs are plotted to compare the various results obtained between the pressure recovery ratio along the cowl and ramp surface for varying angles and concavities. The best pressure recovery attained concurs with literature for a nose cone angle of 11° while its combination with the concavity of 4.318 mm gives the optimum performance.

Keywords
Ramjet Engine, Computational Fluid Dynamics, Pressure recovery ratio, Shockwave and Inlet nose cone.

1. Introduction
Ramjet engine is an air-breathing jet engine that uses the forward motion of the engine to compress the incoming air for combustion. Ramjet engines have the best efficiency at supersonic speed of Mach 3 and are limited to a maximum speed of Mach 6 due to the shockwave-induced pressure loss that occurs due to the slowing of intake air to subsonic speeds. The first part of a ramjet is its diffuser (compressor) in which the forward motion of the ramjet is used to raise the pressure of its working fluid (air) as required for the combustion of fuel. It is then passed through a nozzle to accelerate it to supersonic speeds. This acceleration gives the ramjet a forward thrust. Ramjets cannot produce thrusts at zero speed. Hence, they require an assisted take-off to gain speed until it begins to produce thrust. Inlet cones are a crucial component of Ramjets in raising the pressure inside the engine body, which would eventually produce the thrust. The main purpose of the inlet cone is to slow the flow of air from supersonic flight speed to subsonic speed before entering the engine.

The length of the nose cone assembly and pressure recovery ratio are dependent on nose cone angles. Varying the nose cone angle can result in large number of shockwaves being produced within the body. The optimal nose cone angle provides the best efficiency for its functioning. Ramjets can be particularly useful in applications requiring a small and simple mechanism for high-speed use, such as missiles.

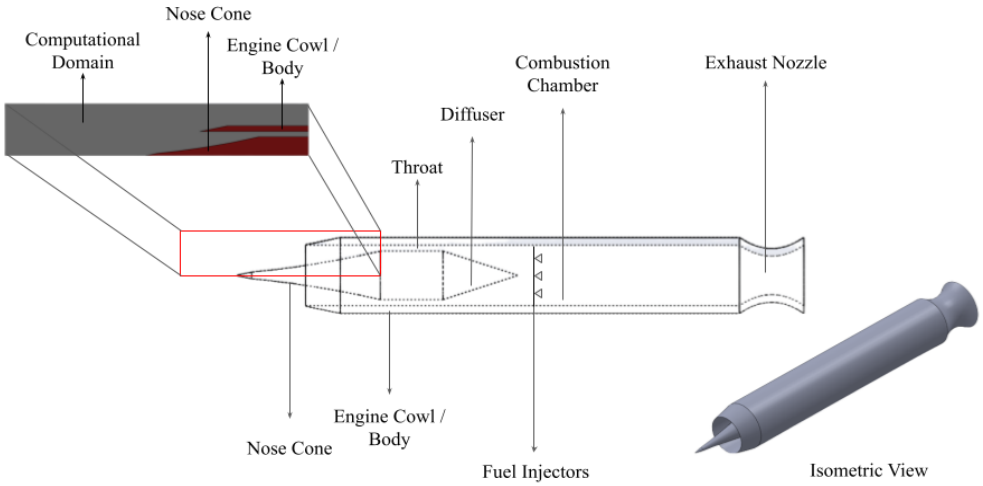

Figure 1. Line diagram and layout of a Ramjet Engine

Figure 1 shows a schematic of a Ramjet engine with the various sections and components labeled. The zoomed-in region (Marked with a red boundary) is the inlet region which is the computational domain for the analysis considered in this study. The air enters the inlet, then passes through the engine cowl and reaches the throat before entering the combustion chamber, where the fuel is burnt and finally released through the exhaust. No spark plugs are required as the compression of gasses heats up the air to self-ignite the fuel. The fuel is provided to the combustion chamber by the fuel injectors. The inlet ramp is responsible for compression of the inlet stream of air while the engine cowl reflects the prescribed shockwaves to contain the high pressures developed along the throat, into the diffuser and subsequently the combustion chamber. The isometric view of the Ramjet engine is shown on the bottom-right corner of Figure 1.
The primary objective of the study is to gauge inlet nose cone performance by measuring the changes in pressure recovery ratio along the length of the engine at various positions. The inlet nose cone angles are varied to understand the conditions which give the best pressure recovery ratio. Further, the concavities are varied at the ramp of the engine until the shockwaves arrive at the cowl tip to provide the best efficiency, as desired. Pressure recovery ratio plots are compared for various angles and concavities to understand the ideal behavior desired for the ramjet engine performance. This study also aims to understand the formation and use of oblique shockwaves in ramjet engines for improving efficiency. Hence, this study focuses on designing and suggesting optimal nose cone angle and geometry for optimal pressure recovery ratio and increased engine efficiency.

2. Literature Review

Several studies are reported about the general concept of a ramjet engine. Verma et al.(2019) studied the inlet isolator geometry of the dual-mode ramjet model, a model with concavities of different depths in the ramp surface to improve performance. This study concluded that 2.54mm and 3.81mm depth concavity in the ramp leads to the formation of additional shockwaves. An increase in mass flow rate is also obtained because of the change in the mode of operation. Kumar et al. (2018) studied that the inlet of a ramjet engine is crucial to its efficiency. Air is better compressed at slower speeds and the inlet cone is responsible for doing the same. Holes along the length of the body of the nose cone further improve the mass flow rate of air and result in an increase in the compression ratio and the efficiency of the engine. The holes also decrease pressure loss through the inlet while increasing the mass flow rate. Akbarzadeh and Karmani (2007) ran simulations of an angled ramp inlet design that produces 3 oblique shockwaves and meets at the engine cowl. Mathematically using Roe Scheme and MacCormac scheme solvers, a total pressure recovery of 0.861 and 0.854 were achieved, respectively. It was noted that when the length of the ramp is longer, it causes more shockwaves to be enclosed within the boundary layer which affects the compression of air at the inlet.
Thangaduraiet al.(2008) simulated the nose cone inlet with cold air flow and heat addition. This study concluded that the air-intake performance is not only affected by its geometry but also by the amount of heat released in the

combustor. Swathi et al.(2018) worked on the analysis of flow over spike and interior of ramjet. Variations of fluid properties such as maximum static temperature at the inlet part of the spike and maximum pressure at the diffuser part of the spike were studied. Wessley and Pardeep (2019) concluded that the thrust generated by the engine increases with an increase in Mach number and the thrust produced by the engine increases with an increase in the inlet area. The findings of Silambarasan and Vivekanandan (2015) were similar to Wessley and Pardeep (2019), where variable inlet areas of ramjet engines were simulated. The study concluded that variation in the mass flow rate of incoming air assists in the production of nozzle exit velocity and thrust value. Khalifa (2021) simulated to show that the inlet back pressure affects the overall pressure recovery. Herrmann et al. (2011) studied boundary-layer bleed where it was noted that, the larger the boundary-layer entrance, the more inlet mass flow is lost and pressure recovery obtained can be increased by raising the subsonic diffuser stepwise. Li et al. (2016) studied the working process of the engine using aluminum powder as the propellant by showing the specific impulse and air-to-fuel ratio for different metals where aluminum achieves the highest specific impulse. Patel et al. (2015) studied that jet velocity for liquid-fueled ramjet is higher than the jet velocity of solid-fueled ramjet. Holst (2012) developed a data reduction method to calculate the engine airflow, net thrust, and specific impulse. Better mixing of air-fuel is done using the swirler which was observed by Arun et al. 2010.

Ferguson et al. (2008) included the use of isometric concepts for the development of supersonic air-breathing configurations, inlet flow field calculations, and estimation of performance at Mach 2 to Mach 6. Ferguson et al. (2009) highlighted the formulae used in this paper for attaining the various design parameters for calculating nose cone angle and prescribed shock angle. Fodeibou et al. (2008) showed that the mass flow rate increases with an increase in the nose cone angle and decreases with an increase in Mach number for a given nose cone angle. Ma et al. (2020) used the C-J detonation theory to predict the pressure in the combustor of scramjets when the combustion flow field is thermal choking and the shock wave is propagating upstream in the isolator. Smart et al. showed that an isolator length design is required to separate the inlet from influences that are moving towards the combustor. Doolan (2006) theoretically shows that hydrocarbon fuels that have lower heating values and high density can have losses in mixing which is dominant in supersonic combustors. Kamali et al. (2015) showed that at a higher Mach number, the distance between the first and second shock wave goes up to show higher strength of the shock. From the details of the literature mentioned above, all the studies refer to the functioning of the ramjet engine with respect to one of the parameters. In order to fill up the gap in the literature, the present study aims at providing an analysis of the combined effects of nose cone angle and concavities.

3. Methodology

To understand the effect of various nose cone geometries on the performance of the inlet of a ramjet engine, a Computational Fluid Dynamics (CFD) analysis is done. The analysis for various cases is conducted on "SCFLOW", a CFD tool that uses unstructured/polyhedral meshes to represent complex geometries and ensures better interaction of neighboring elements during a fluid flow scenario. The use of a density-based solver allows us to better visualize the changes in pressure and volume as the gasses get compressed within the domain. Figure 2a shows the various regions and parts in a ramjet engine's inlet. The Figure shows the formation of the prescribed shockwave which is the shockwave formed by the nose cone tip and is crucial to the performance of the engine's inlet as it directly affects the pressure recovery of the engine.

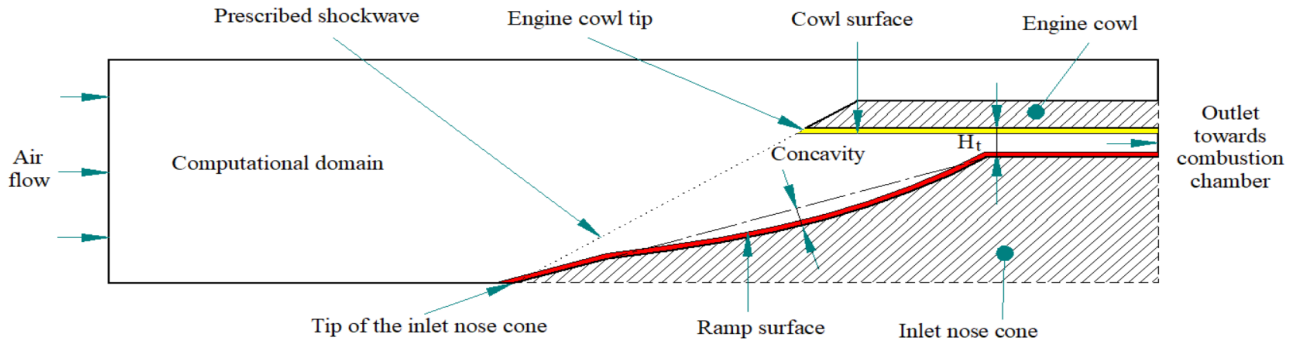

Figure 2a: Half-section schematic of the nose cone inlet

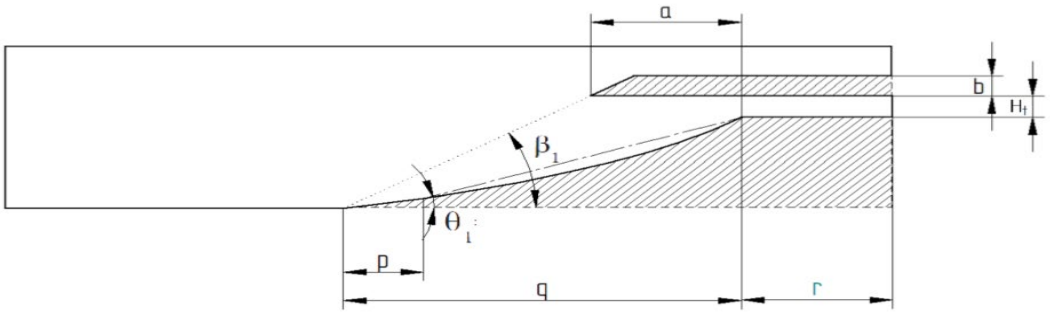

Figure 2b: Dimensional notations of the nose cone inlet

In Figure 2b. the dimensions for the corresponding notations in the validation case are as follows:
Distance between the nose cone tip and concave region **(p)**= 25.44 mm
Length of the compression lamp **(q)** = 248.158 mm
Length of isolator region **(r)** = 88.392 mm
Distance from engine cowl tip to isolator region **(a)** = 111.76 mm
Height of throat **(H_t)** = 10.16 mm
Thickness of cowl **(b)** = 12.7 mm
Concavity = 3.81 mm **(0.15 in)**
A concave section is added along the inlet compression ramp to further improve the pressure recovery as found in Verma et. al(2019).A CAD model with the above dimensions is designed on "SOLIDWORKS". The 2D profile shown in Figure 2 is then extruded to a thickness of 5.08mm. The design is considered in such a way so as to ensure that the boundary conditions and the general setup of the simulation is in-line with the literature. Once established that the results obtained from the CFD program are matching the results obtained in the literature, all subsequent cases use the same boundary conditions which are as follows:

Table 1. Boundary Conditions for the analysis

Parameter	Value	Description
Analysis Type	Heat and Turbulent Flow, RANS SST k-ω model, Steady-state analysis	The SST k-ω shows good behavior in adverse pressure gradients and separating flow, allowing the effect of shockwaves to be better accounted for in the pressure contours.
Domain material	Air, Compressible	Relationship between pressure and density is significant at Mach number >0.8 and cannot be observed with incompressible flow analysis.
Solver	Density-Based Solver	Pressure is a function of density in a compressible flow, which is not accounted for in pressure-based solvers.
Initial/Free Stream Flow Velocity	Mach 4.03	Supersonic Flow
Initial/Free Stream Temperature	69.15 K	As per literature
Initial/Free Stream Pressure	8724 Pa	Pressure at an altitude of 17,000m

3.1 Varying the Nose Cone Angle (θ_1)

To gauge the performance of different geometries of a ramjet engine's inlet, nose cone angles are varied. Based on the nose cone angle, the shock angle is calculated, and the cowl tip is designed to coincide with the prescribed shockwave with the following formula:

$$tan\ \theta_1 = 2\ cot\ \beta_1 \frac{{M_\infty}^2 sin^2\beta_1 - 1}{{M^2}_\infty(\gamma + cos\ 2\beta_1)+2} \quad (1)$$

Where:

- θ_1 is the nose cone angle (6° to 20°)
- β_1 is the prescribed shock angle (to be calculated)
- M_∞ is the cruise Mach Number = 4.03
- $\boldsymbol{\gamma}$ is the ratio of specific heat at constant pressure to specific heat at constant volume (C_p/C_v) = 1.5

Angle of the nose cone is varied from 6° to 20° in increments of 2°. The prescribed shock angle (β_1) is calculated accordingly, and the cowl is designed to coincide with the prescribed shockwave. A simulation case with the boundary conditions as described in Table 1 is conducted. After the simulation case, in the post-processor, points are plotted at three positions, along the inlet/compression ramp - on the nose cone tip, start of the isolator region and at the throat to obtain the variation in static pressure along the surface. The same is repeated for the inner cowl surface. This data is tabulated and graphs are plotted to analyze the trends. The nose cone angle which induces the highest-pressure recovery is chosen.

3.2 Varying the concavity of the inlet ramp

Considering the nose cone angle with the highest-pressure recovery, the subsequent designs keep θ_1 constant with variations in the concavity. The cowl length too remains constant. The concavities are varied from 2.794 mm to 4.826 mm in increments of 0.508 mm (0.02 in). Varying the concavity of the inlet ramp has shown to improve its compression performance, as found in Verma et al.(2019). CAD models for the respective dimensions are made on SOLIDWORKS and simulations with boundary conditions as listed in table 1 are conducted. To get the variation in pressure along the surface, points are plotted at three locations - on the nose cone tip, start of the isolator area, and the throat. The same is repeated for the inner cowl surface. To assess the trends, the data is tabulated and graphs are plotted.

4. Data Collection

Using the formula described in the methodology section, keeping $\boldsymbol{\gamma}$ = 1.5 and M_∞= 4 as constant, for variations in θ_1° from 6° to 20°, the following results as described in table 2 are obtained. These are used in the design of various ramjet inlet nose cones that are depending upon the nose cone angle and the prescribed shock angle.

Table 2. Data calculated using the numerical formulae

$\boldsymbol{\gamma}$ (Heat Capacity Ratio)	M_∞ (Free stream Mach number)	θ_1° (Nose Cone Angle)	β_1° (Principal shock angle)	M_1 (Mach Number behind principal shockwave)
1.5	4	6	19.02	3.49
1.5	4	8	20.771	3.33
1.5	4	10	22.6345	3.17
1.5	4	11	23.535	3.11
1.5	4	12	24.608	3.01
1.5	4	14	26.688	2.85
1.5	4	16	28.873	2.69

1.5	4	18	31.165	2.54
1.5	4	20	33.562	2.38

In Table 2, consolidated results of prescribed shock angles at varying inlet nose cone angles are present. Here, $\boldsymbol{\gamma}$ is the ratio of specific heat at constant pressure to specific heat at constant volume (C_p/C_v), M_∞ is cruise Mach number, θ_1 is the inlet nose cone angle, β_1 is prescribed shock angle, and M_1 is Mach number behind the shock.

5. Results and Discussion

In this section, variations in nose cone angles and concavities are considered and results are compared with each other using the pressure recovery ratio plots and pressure contours at ramp and cowl surfaces. Initially, validation is conducted in order to determine the ideal boundary conditions, and the same setup is used in the study for the further set of simulations.

5.1 Validation

In order to validate the setup in the present study, simulations were performed to obtain the results in accordance with that of Verma et al.(2019). Here, the computation is carried out on the inlet nose cone of 11° with a concavity of 3.81 mm**,** designed as per the literature. The input parameters including the boundary conditions were defined in accordance with the literature. Figure 3 represents the pressure contours for the set conditions.

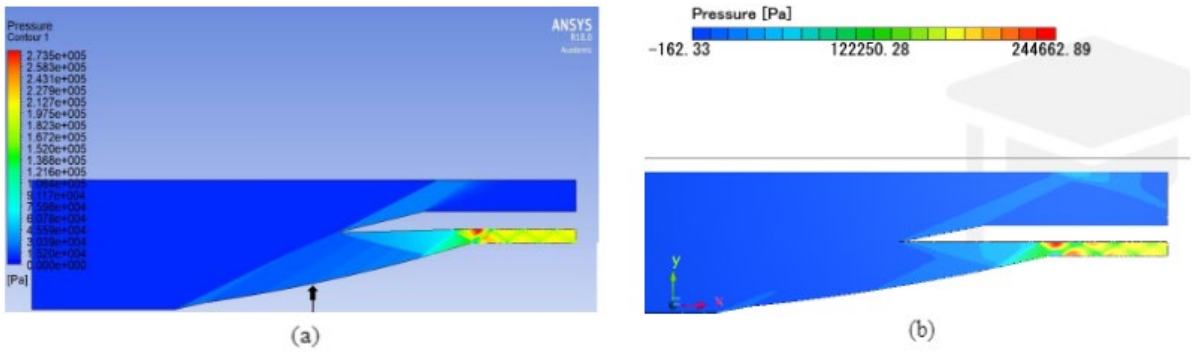

Figure 3. Pressure contour for (a) results of Verma et al. (2019) and (b) results of the present study

Figure 3(a) shows the simulation results of Verma et al. (2019) while their corresponding results from the present study are shown in Figure 3(b). It can be seen that the obtained results are in good agreement with the literature.

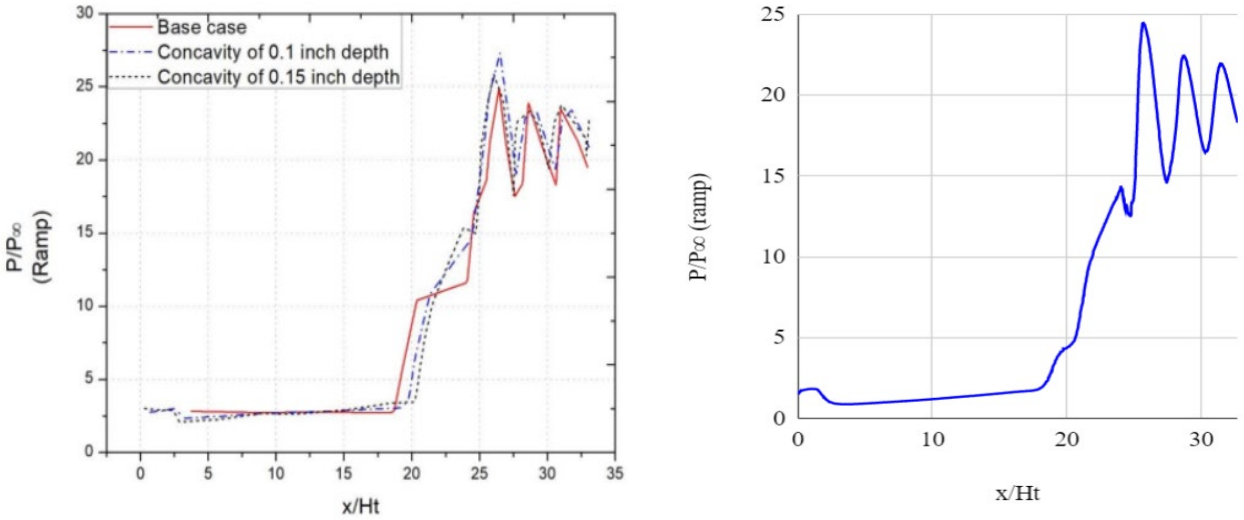

(a) (b)

Figure 4. Pressure recovery ratio along ramp surface for (a) simulation results of Verma et al.(2019) and (b) results of the present study

Figure 4 shows pressure recovery ratio against x/H_t along the ramp surface, where x/H_t is the ratio of horizontal distance of a specified point from the tip of the nose cone (x) to the height of the throat (H_t). The pressure recovery ratio (P/P_∞) obtained from the simulation results of the current study is in line with the one obtained from the literature. The peak pressure recovery ratio in both the cases is found at a common point and the peak pressure is obtained along the cowl region. It can be observed from the graphs shown in the Figure, that the pressure recovery ratio follows the same trend. The peak pressure values reach local maximum and minimum as the shockwave propagates within the ramjet inlet. The points of maxima and minima can be verified along the ramp and cowl surface. In this configuration, the peak pressure recovery ratio along the ramp surface is close to 26, obtained at an x/H_t value of around 27.

The trend shown in Figure 4(b) is for the pressure recovery ratio along the ramp surface of the present study, which is in good accordance with the results obtained by Verma et al. (2019). The initial pressure recovery ratio drop for the case of 3.81 mm in the present study and literature results is obtained at an x/H_t value of around 26. The variations follow similar trends in the case of pressure distribution along the ramp and cowl. It is important to note that the values in the two studies would not form a one-to-one correspondence owing to dissimilarity in the capabilities of the software being used.

5.2 Variation of inlet nose cone angle

The combustion performance and overall efficiency of a ramjet intake depend on the pressure recovery ratio. As per results obtained by Kumar et al. (2018), pressure recovery is dependent on the inlet nose cone angle. Hence, the performance of varying inlet nose cone angles is studied in terms of pressure recovery. The graphs of pressure recovery ratio v/s x/H_t for the inlet nose cone angle 6°, 8°, 10°, 11°, 12°, 14°, 16°, 18°, and 20° are studied. In general, the pressure recovery ratio is studied along the ramp and cowl surfaces.

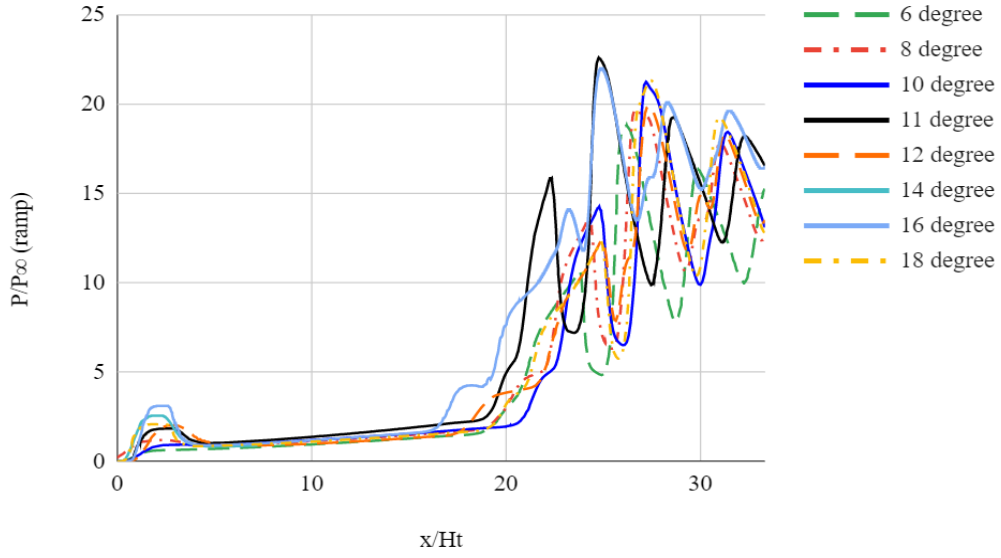

Figure 5. Consolidated pressure recovery ratio curves along ramp surface for various inlet nose cone angles

Figure 5 represents the pressure recovery ratio curve for the ramp surface with x/H_t for various inlet nose cone angles. From the trend shown, it can be noted that the pressure recovery ratio is maximum for the 11° nose cone angle with a value of 22.5. The pressure recovery ratio of 6° nose cone angle is the least with a magnitude of 18.8. The pressure recovery ratio increases with the increase in the nose cone angle due to the generation of more secondary shockwaves.

The pressure recovery ratio value decreases after reaching 11° as the primary shockwave is converging and does not hit the cowl tip as designed.

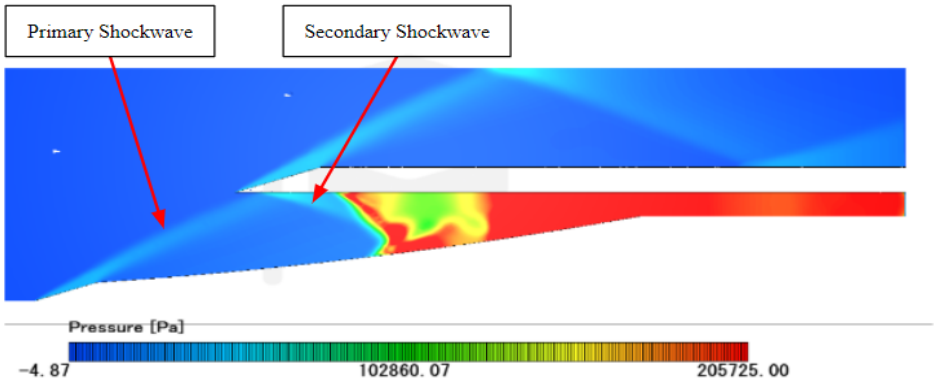

Figure 6. Pressure contour for simulation results of 20° nose cone angle.

Among the obtained results, the nose cone angle at 20° (Figure 6) shows clear failure as the prescribed shockwave is unable to hold the backpressure within the isolator region. The high back pressure causes the heated air to leak out of the inlet region, reducing system efficiency and causing several regions of an aerodynamic stall. This sets a limit on the nose cone angle to 18° for the considered model. Hence, the values obtained from the 20° case are omitted from the plotted graphs.

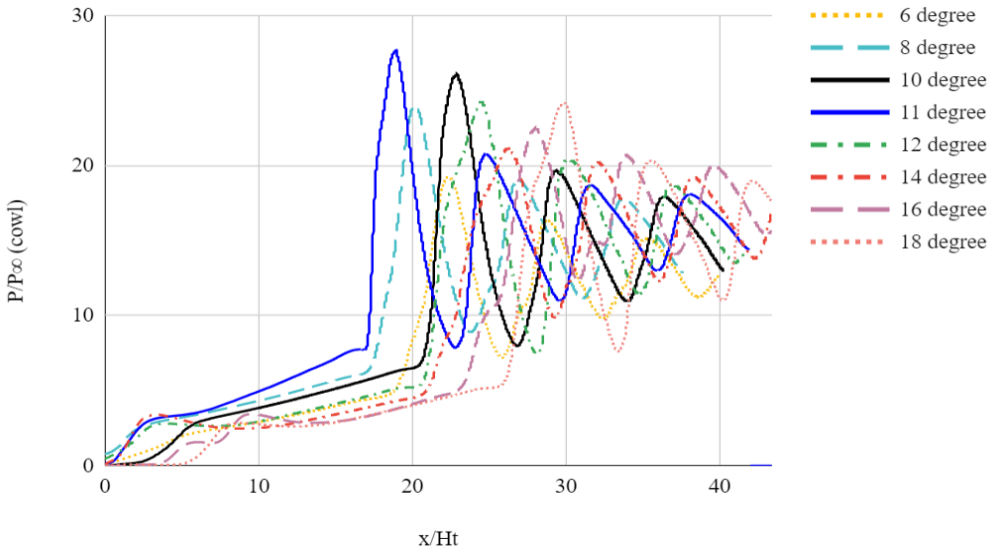

Figure 7. Consolidated pressure recovery ratio curves along the cowl surface for various inlet nose cone angles

Figure 7 represents the pressure recovery curves along the cowl surface for various inlet nose cone angles. It can be noted that the pressure recovery ratio is maximum for the 11° nose cone angle with a value of 27.5. The pressure recovery ratio of the 6° nose cone angle is the least, having a value of 19.2. This occurs due to an increase in the number of secondary shockwaves. Here, values obtained from the 20° case are omitted from the plotted graphs due to the observation of several regions of an aerodynamic stall for the same. As per the above analysis, the maximum pressure recovery ratio is being obtained for the inlet nose cone angle of 11°. It is also noted from plots of cowl and ramp surfaces for any given angle, that the value of pressure recovery obtained along the cowl surface is more than that obtained along the ramp surface. Hence, the best combustion performance and overall efficiency of a ramjet intake are obtained at the inlet nose cone angle of 11°.

5.3 Variation of concavity

In this section, we study the variation in pressure recovery ratio with changes in the concavity along ramp and cowl surfaces, respectively. These plots can be used to determine the best pressure recovery ratio case. The graphs of pressure recovery ratio v/s x/Ht for the inlet nose cone angle of 11° at varying concavities are studied. In general, the pressure recovery ratio is studied along the ramp and cowl surfaces.

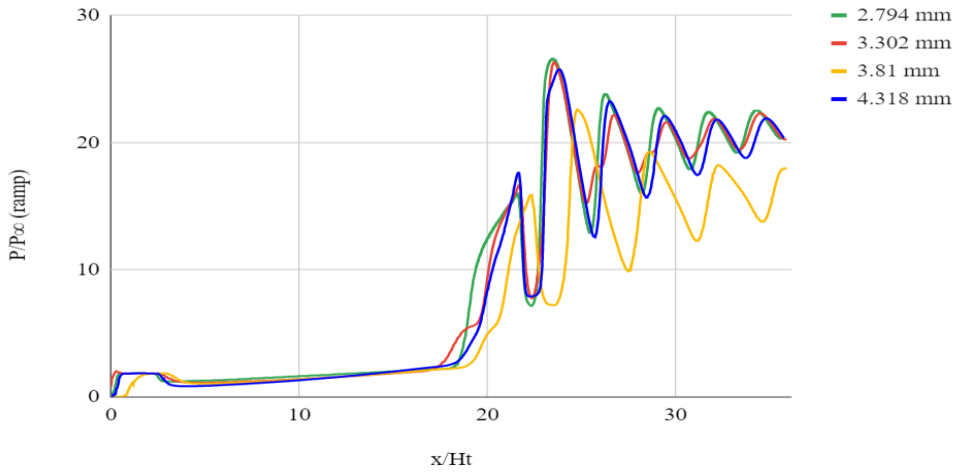

Figure 8. Consolidated pressure recovery ratio curves along the ramp surface for various concavities at 11° nose cone angle

Figure 8 represents the pressure recovery ratio curves along the ramp surface for the inlet nose cone angle of 11° at different concavities. It can be noted that the pressure recovery ratio is maximum for the concavity of 2.794 mm with a value of 26.5. The pressure recovery ratio at a concavity of 3.81 mm is the least with a magnitude of 22.4. The pressure recovery ratio value for concavities of 2.794 mm, 3.302 mm and 4.318 mm are very close, with 4.318 mm being the highest.

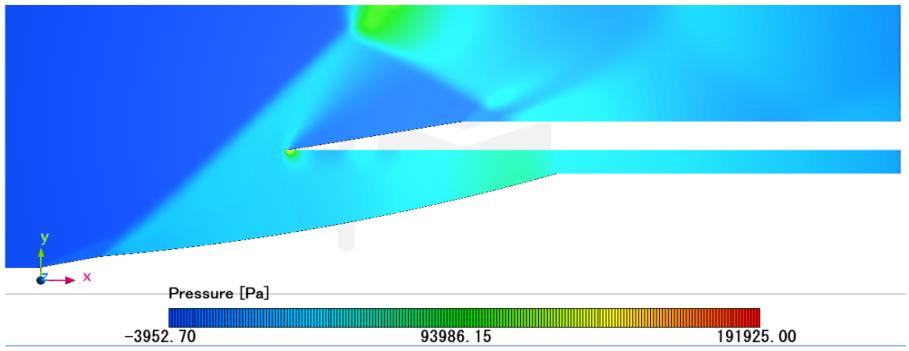

Figure 9. Pressure contour for the concavity of 4.83 mm.

For the case having a concavity of 4.83 mm (Figure 9), high back pressure causes the heated air to leak out of the inlet region, leading to an aerodynamic stall. Hence, the values obtained from the case with a concavity of 4.83 mm are omitted from the graph.

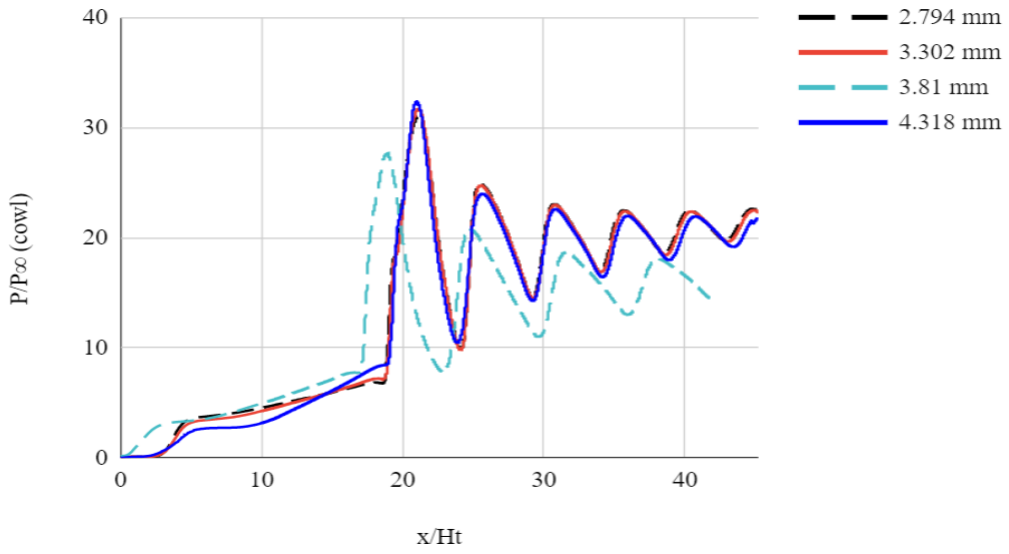

Figure 10. Combined pressure recovery ratio curves along cowl surface for various concavities at 11° nose cone angle

Figure 10 represents the pressure recovery ratio curves along the cowl surface at varying concavities. It can be noted that the pressure recovery ratio is maximum for the 11° nose cone angle with a concavity of 4.318 mm having a value of 32.5. The pressure recovery ratio for the concavity of 4.318 mm nose cone angle is the least with a magnitude of 27.5. The pressure recovery ratio value for concavities of 2.794 mm, 3.302 mm and 4.318 mm are very close, with 4.318 mm being the highest. On careful observation, it is concluded that the maximum pressure recovery ratios are obtained for the inlet nose cone angle of 11° with a concavity of 4.318 mm and 2.794 mm along the cowl and ramp surfaces respectively. Since the value of pressure recovery obtained along the cowl surface is more than that obtained along the ramp surface, the maximum pressure recovery to be along the cowl surface is considered.

5.4 Pressure Contours

In this section, we study the pressure contours obtained from the CFD simulation of the inlet nose cone angle of 11° with a concavity of 4.318 mm. The study of this contour helps to reveal the pattern in which the primary and secondary shockwave generates and propagates within the isolator region. This propagation leads to the generation of high-pressure zones around the shockwave.

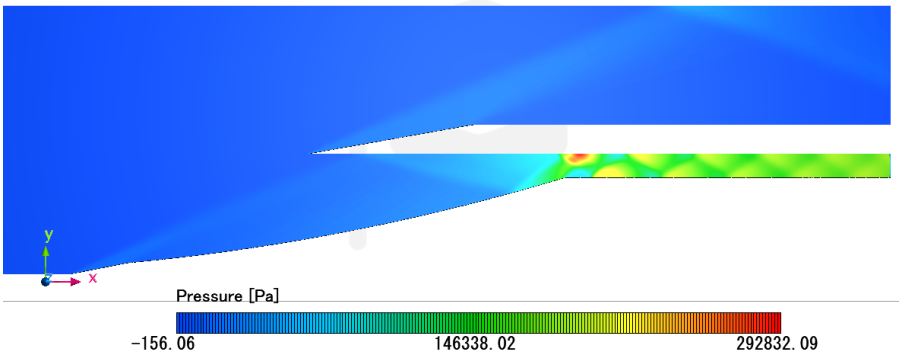

Figure 11. Pressure contour for 11° nose cone having concavity of 4.318 mm.

Figure 11 represents the pressure contours for the 11° nose cone angle at 4.318 mm concavity. The different colors represent the intensity of pressure levels within the domain. All the colors correspond to the pressure values specified in the legend. Here, the shockwave propagation along the isolator region can be clearly seen, with the maximum pressure region being generated along the cowl region. The maximum pressure value at the cowl surface is 292832.09

Pa. It is also noted that the primary shockwave gets converged with secondary shockwaves, due to which the primary shockwave is not hitting the cowl at the cowl tip.

6. Conclusion

Considering the advent of research in the field of Ramjet Engines, this paper describes the effect of varying inlet nose cone angles and concavities on pressure recovery ratio. Initially, the model geometry is considered by varying the inlet nose cone angles from 6° to 20° in steps of 2°. Upon selection of the ideal nose cone angle, the best configuration is suggested by analyzing the performance of the nose cone angle at various concavities. The concavity is varied from 2.794 mm to 4.826 mm in the steps of 0.508 mm.

The inlet nose cone angle of 11° is used to validate the model by simulating the setup suggested in the literature. The boundary conditions mentioned in the literature are applied in the simulations. The obtained pressure recovery ratio plots and pressure contours fall in good agreement with the literature results. The same setup is used for the study of configurations with variable nose cone angles. It is noted that high back pressure in case of 20° causes the heated air to leak out of the inlet region, reducing system efficiency and leading to an aerodynamic stall. With respect to the effect of angle, it can be concluded that the 11° nose cone angle has the best pressure recovery ratio. The results obtained from variable nose cone angles are further extended to note the effects of variable concavity. The concavity of 3.81mm was suggested in the literature. The effects of various concavities, ranging from 2.794 mm to 4.826 mm, are investigated in this study. It is found that an aerodynamic stall is obtained in the case of 4.826 mm. Importantly, in the present study, it is noted that a concavity of 4.318 mm gave the best pressure recovery at 11° nose cone angle. It can be concluded that variation in inlet nose cone angles leads to non-monotonic changes in pressure recovery ratio. At a smaller nose cone angle, lesser number of secondary shockwaves are being produced and as a result, the primary shockwave hits the cowl tip. Since the number of primary shockwaves being produced are less at smaller nose cone angles, the pressure recovery ratio is low. With an increase in the size of concavity, the number of secondary shockwaves increases, and hence the pressure recovery also increases. But at large nose cone angles ($\theta_1 > 11°$), more number of secondary shockwaves deflect the primary shockwave within the cowl surface. As a result, overall shockwave propagation is disturbed due to the deflections, reducing the pressure recovery ratio. Also, the presence of concavity along the ramp surface alters the flow leading to a total pressure rise in the concavity models. Hence, with the increase in concavity, a gradual increase in the pressure recovery ratio is observed.

Proposed Improvements

Further improvements to precisely gauge the pressure recovery ratio by considering the addition of the diffuser at the inlet nose cone. While the compression ramp and isolator region play a significant role in compressing the inlet stream of air, the diffuser further contributes to the pressure recovery ratio. A study on the design of the diffuser in the inlet nose cone would suggest the ideal geometry for supersonic applications.

References

Akbarzadeh, M. and Karmani, M.J., Numerical computation of supersonic-subsonic ramjet inlets; a Design Procedure, *15th. Annual (International) Conference on Mechanical Engineering-ISME, 2007,* Amirkabir University of Technology, Tehran, Iran, 15-17May 2007.

B, Arun., A.K, Manoj.kumar., B, Silambarasan., Abdullah, Mohammed. And Chand, Dharmahinder.Singh., Performance study of ramjet using swirler, *13th Asian Congress of Fluid Mechanics* ,Dhaka, Bangladesh., December, 2010.

Doolan, Con.J., An air-launched hypersonic vehicle performance model, The University of Adelaide, South Australia, Australia, 2006.

Ferguson, Frederick., Dhanasar, Mookesh., Blankson, Isaiah.M. and Kankam, David., Supersonic and hypersonic slender air-breathing configurations derived from 2d flowfields, *46th AIAA Aerospace Sciences Meeting and Exhibit*, Reno, Nevada , 07-10 January, 2008.

Ferguson, Frederick., Dhanasar, Mookesh., Blankson, Isaiah.M., Preliminary design of a tip-to-tail model of a ram-scramjet engine, *47th AIAA Aerospace Sciences Meeting including the New Horizons Forum and Aerospace Exposition,* Orlando, Florida, DOI:10.2514/6.2009-714, January, 2009.

Fodeibou,Taher., Huque, Ziaul. And Galvis, Jenny., Effects of mach number and angle of attack on mass flow rates and entropy gain in a supersonic inlet, *World Academy of Science, Engineering and Technology,* June, 2008.

Herrmann, Dirk., Blem, Sergej. And Gülhan, Ali., Experimental study of boundary-layer bleed impact on ramjet inlet performance, *Journal of Propulsion and Power,* vol. 27., no. 6., November – December, 2011.

Holst, Kevin.Raymond., A method for performance analysis of a ramjet engine in a free-jet test facility and analysis

of performance uncertainty, *A Thesis Presented for the Master of Science Degree,* The University of Tennessee, Knoxville., May, 2012.

Kamali, Reza., Mousavi, Seyed.Mahmood., Binesh, Ali.Reza.,Three dimensional CFD investigation of shock train structure in a supersonic nozzle, *Acta Astronautica S0094-5765(15)00269*., 6 June, 2015.

Khalifa, Abdelmola.Albadwi.Al., Design and analysis of an air intake system of ramjet engine using cfd simulations, *International Journal of Engineering and Information Systems (IJEAIS) ISSN: 2643-640X ,* vol. 5., issue 2., pp 180-190., February, 2021.

Kumar, G.Dinesh., Gowrishankar, D. and Suresh, C., Numerical analysis of ramjet spike with various cone angles, *International Journal of Pure and Applied Mathematics,* vol. 119., no. 15., pp. 233-245., 2018.

Li, Chao., Hu, Chunbo., Xin, Xin., Li, Yue. And Sun, Haijun., Experimental study on the operation characteristics of aluminum powder fueled ramjet, *ActaAstronautica,* vol.129, pp. 74-81.,December, 2016

Ma, Kaifu., Zhang, Zijian., Liu, Yunfeng. And Jiang, Zonglin., Aerodynamic principles of shock-induced combustion ramjet engine, *Aerospace Science and Technology,* vol. 103., August, 2020.

Patel, Murlidhar., Sen, Prakash.Kumar., Sahu, Gopal. And Sharma, Ritesh., A review on ram jet engine, *International research journal (IRJ) e-ISSN: 2348-6848, p- ISSN: 2348-795X,* vol. 2., issue 11., November, 2015.

Professor Smart, Michael.K., Scramjet Isolators, RTO-EN-AVT-185, The University of Queensland Brisbane,AUSTRALIA

Silambarasan, R. and Dr. Vivekanandan, R., Computational fluid dynamic analysis of variable inlet area ramjet engine, *International Journal of Research and Innovation in Engineering Technology ISSN: 2394 – 4854,* vol. 01., issue 10., pp. 1-5., March, 2015.

Swathi, Guthula., Snigdha, M., Sravanthi, G.andAlekya, B., Cold flow analysis of flow over a ramjet engine, *International Journal of Mechanical and Production Engineering Research and Development (IJMPERD) ISSN (P) 2249-6890;*vol. 8 issue 4., pp. 9-14., Aug. 2018.

Thangadurai, G.Raja.Singh., Chandran, B.S.Subhash., Babu, V. and Sundararajan, T., Numerical analysis of integrated liquid ramjet engine, *Defense Science Journal,* Vol. 58 No. 3., pp. 327-337 .,May 2008.

Verma, Rahul., Shukla, Alokita., Raj, R.Thundil.Karuppa. and P, Senthilkumar., Numerical simulation of supersonic flow through inlet isolator dual mode scramjet model with concavity in ramp, *Conference AIAA aviation forum 2019,* DOI:10.2514/6.2019-3221, Texas, USA, June 14, 2019.

Wessley, G.Jims.John. and Pardeep, Shilpa., Parametric analysis of a dual combustion ramjet engine, *International Journal of Recent Technology and Engineering (IJRTE) ISSN:2277-3878,* vol.7, issue 64., April, 2019.

Biography

Dr. Avinash Govindraju is assistant professor in the department of mechanical engineering, BMS Institute of Technology & Management. He is a masters and PhD graduate from IIT Madras with specialization in thermal sciences - Thermodynamics & Combustion. He worked in KLA-Tencor for a year. He is skilled in programming using Python and Fortran, Basics of MATLAB, C, C++. He is also skilled in software packages such as SOLIDWORKS, FDS, ANSYS FLUENT, CATIA, PRO-E, and Big Data softwares including MySQL, PostgreSQL.

Dr. Santosh Kumar is assistant professor in the department of mechanical engineering, BMS Institute of Technology & Management. He earned his masters and PhD from IISc Bangalore. His areas of expertise include Mechanical sheet metal joining, Friction Stir Welding (FSW), Tribology, Simulations, Design of rivets for novel joining methods. SEM, 3D Profilometer.

Tarun Pachauri, Kartikay Awasthi, Nihal. U. Shetty, Vipan Singh and Karan Manoj are undergraduate student in the department of mechanical engineering, BMS Institute of Technology & Management.